# Size-selective concentration and label-free characterization of protein aggregates using a Raman active nanofluidic device†

Inhee Choi,[a] Yun Suk Huh[ab] and David Erickson*[a]

*Received 6th September 2010, Accepted 10th November 2010*
**DOI: 10.1039/c0lc00383b**

Trace detection and physicochemical characterization of protein aggregates have a large impact in understanding and diagnosing many diseases, such as ageing-related neurodegeneration and systemic amyloidosis, for which the formation of protein aggregates is one of the pathological hallmarks. Here we demonstrate an innovative label-free method for detecting and characterizing small amounts of early stage protein aggregates using a Raman active nanofluidic device. Sub-micrometre channels formed by a novel elastomeric collapse technique enable the separation and concentration of matured protein aggregates from small protein molecules. The Raman enhancement by gold nanoparticle clusters fixed below a micro/nanofluidic junction allows characterization of intrinsic properties of protein aggregates at concentration levels (~fM) much lower than can be done with traditional analytical tools. With our device we show for the first time the concentration dependence of protein aggregation over these low concentration ranges. We expect that our method could facilitate definitive diagnosis and possible therapeutics of diseases at early stages.



## 1 Introduction

The extracellular and/or intracellular formation of protein aggregates, in the form of amyloid fibrils and disordered or amorphous structures, are one of the pathological hallmarks shared by many diseases including ageing-related neurodegeneration and systemic amyloidosis. Among them, neurodegenerative diseases, such as Alzheimer's disease (AD), Parkinson's disease, Huntington's disease, Prion diseases, and amyotrophic lateral sclerosis (ALS), are increasingly being identified as having common cellular and molecular mechanisms including protein aggregation and inclusion body formation.[1–3] As a result, trace detection and physicochemical characterization of protein aggregates can have a large impact in understanding and diagnosing diseases at early stages.

Towards this end, multiple analytical methods including size exclusion chromatography,[4,5] dynamic light scattering,[4,6] fluorescence spectroscopy,[4,6–8] circular dichroism (CD) spectroscopy,[4,7–9] and nuclear magnetic resonance (NMR) spectroscopy[9–11] have been employed to characterize the protein aggregation process. While all these techniques are functional, it remains extremely challenging to detect and characterize protein aggregates at very low concentrations. The reasons for this include: restricted applicability of small[4,5,12] or crystallizable[9–12] protein aggregates, non-uniform distribution in a sample,[4,6–9,12] challenging labeling procedures,[4,6–8,12] and the poor sensitivity of existing analytical tools.[4–12]

To selectively separate protein aggregates from their native protein, ultracentrifugation methods with filters can be useful. However, these methods have possibility to collect much more aggregates than an initial amount of protein aggregates in a sample. This is due to the fact that centrifugation[13] and the resulting temperature increase[6] can induce the unintentional precrystallization and/or aggregation in protein solutions. And this pretreatment method requires an additional process to re-suspend separated protein aggregates into a buffer for further analyses to characterize protein aggregates.

To overcome these limitations, we have developed a Raman active nanofluidic device that enables size-selective concentration and simultaneous label-free characterization of protein aggregates at fM levels. Our approach is illustrated schematically in Fig. 1. As a sensing principle, we have adopted surface-enhanced Raman scattering (SERS), which provides a significant enhancement of the typically weak Raman signal intensity through a series of electromagnetic field and chemical enhancements induced by the adsorption of molecules onto irregular metal surfaces.[14] SERS spectroscopy is an extremely powerful tool for obtaining information on protein structures; however, it requires that samples be selectively concentrated at a site where the optical field can be locally enhanced through the generation of a surface plasmon. To achieve this, our device fuses a micro/nanofluidic junction formed by elastomeric collapse (Fig. 1a) with a gold nanoparticle based SERS active surface (Fig. 1b). To demonstrate our device, we examined Cu/Zn-superoxide dismutase (SOD1) aggregates. SOD1 aggregates were selected as targets for this study, since they have been strongly implicated as causative factor in ALS (*i.e.* Lou Gehrig's disease[4–10,15–19]) and have been observed in both amyloid fibril and amorphous

[a]*Sibley School of Mechanical and Aerospace Engineering, Cornell University, Ithaca, NY, 14853, USA. E-mail: de54@cornell.edu; Fax: +1 607-255-1222; Tel: +1 607-255-4861*
[b]*Division of Materials Science, Korea Basic Science Institute, Daejeon 305-333, Korea*

† Electronic supplementary information (ESI) available: A demonstration of size-selective concentration of PS beads with different diameters, a comparison of fluorescence signals obtained from nanofluidic device with traditional fluorescence analysis, and characterization results of changes in structural and superficial properties by SOD1 aggregation were provided. Experimental details and another application result of nanofluidic concentration device to Aβ protein aggregates were also provided. See DOI: 10.1039/c0lc00383b

 

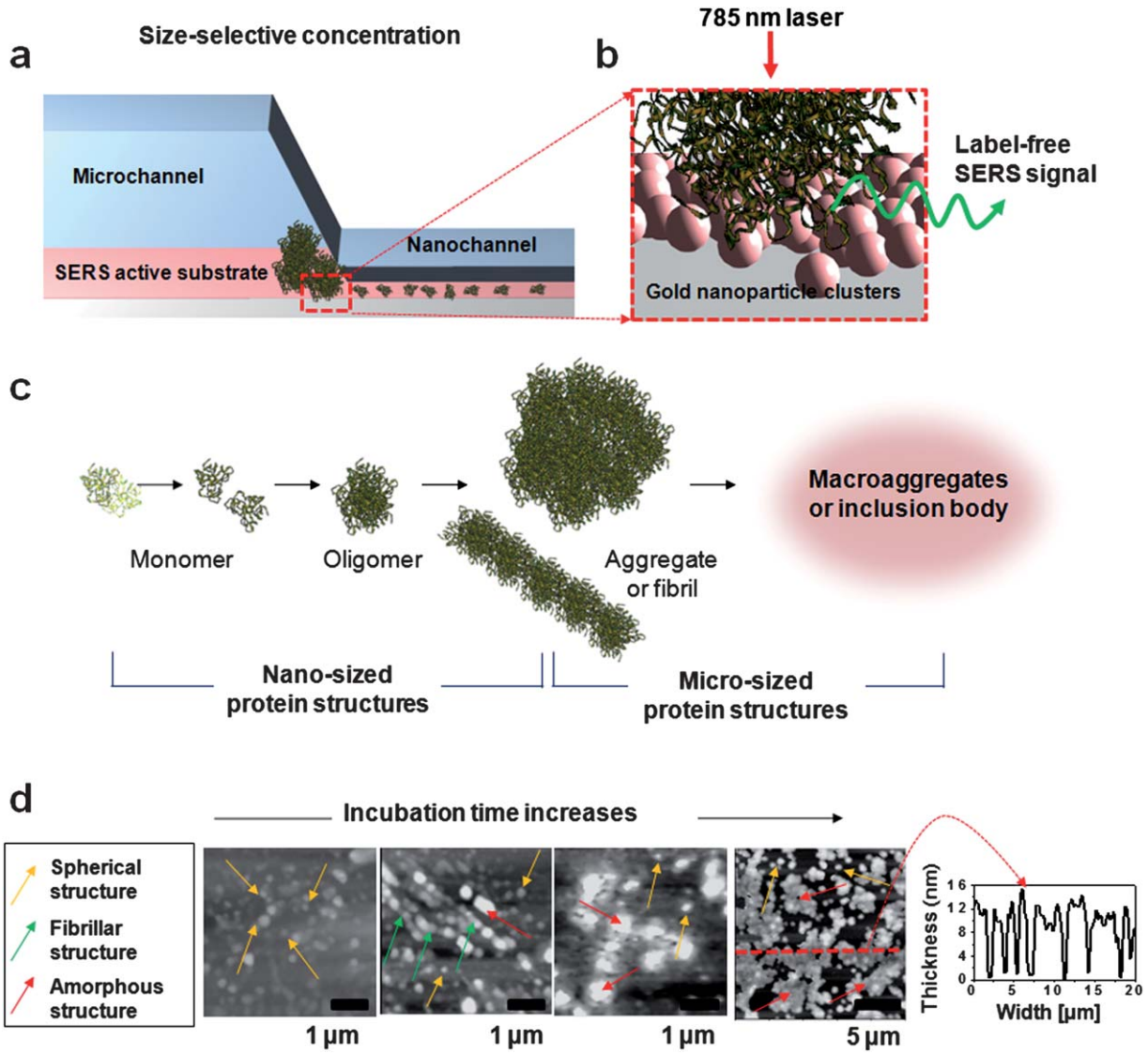


**Fig. 1** Schematic diagram for the concentration and detection of protein aggregates. (a) Illustration of a fluidic junction between a microchannel and a nanochannel for the size-selective concentration of protein aggregates. (b) Close up view of the protein aggregates near the SERS active substrate used for label-free Raman detection. (c) General mechanism of protein aggregation. (d) Time-resolved AFM imaging of SOD1 aggregation. Incubation time was from 2 to 5 days (left to right). Colored arrows indicate various aggregate structures as described in the legend.

aggregate forms in tissues from ALS transgenic bodies as well as *in vitro* studies.[4–8,10,15–17]

Fig. 1c shows the general growth process for SOD1 aggregates which have been characterized extensively in the literature.[1,3,4,18] Using time-resolved morphological imaging under destabilizing conditions, SOD1s can be seen to undergo a transition from small spherical structures to large aggregates including amorphous structures and some fibrillar structures (Fig. 1d). These structures are considered as intermediates during the formation of inclusion body. Recently, these types of intermediates have been hypothesized to be more toxic than either the precursor protein or micro-sized aggregates and inclusion body.[1,2,4,6,9,15] Other data suggest that small SOD1 aggregates with nanometre scale dimensions appear in transgenic mouse spinal cords alongside the onset of ALS symptoms.[1,15,17,19] In this study, we designed a nanofluidic device that can concentrate the intermediates of SOD1 aggregates including nano-sized structures, to effectively separate and detect SOD1 aggregates with toxic implication at the early stages. The intrinsic properties of the selectively concentrated SOD1 aggregates were characterized by collecting label-free Raman spectra. Our results demonstrate the ability of a Raman active nanofluidic device to perform trace detection and physicochemical characterization of protein aggregates with the sizes implicated in diseases, irrespective of their solubility, morphology, and crystallinity.

## 2 Materials and methods

### 2.1 *In vitro* formation of protein aggregates

SOD1 extracted from human erythrocytes (Sigma) was diluted with a phosphate buffer saline (PBS) solution at various concentrations

ranged from 3 fM to 300 nM. *In vitro* formation of SOD1 aggregates was performed by adding a 2,2,2-trifluoroethanol (TFE) solution to the diluted SOD1 solution with TFE volume ratio (v/v) of 20%. To identify aggregate formation, each sample was added to 30 μM ThT in PBS with volume ratio of 1 : 10, and ThT fluorescence of samples was measured by microplate spectrofluorometer (Gemini EM-Molecular Devices) with excitation and emission wavelengths of 435 and 480 nm, respectively.

### 2.2 Fabrication of a Raman active nanofluidic device

To begin the fabrication of the nanofluidic channels (Fig. 2), the desired pattern was made on a silicon wafer using standard photolithography processes. Negative photoresist SU-8 (Microchem) 2000.5 (for a nanochannel) and 2010 (for a microchannel) were used to create the different heights of the master. The polydimethylsiloxane (PDMS) base to curing agent ratio was 10 : 1 by weight. After mixing the curing agent and elastomer base and degassing the mixture, it was cast onto the premade master and allowed to cure at 80 °C for 4 hour. After the PDMS mold was removed from the master, it was bonded to a SERS active substrate by plasma oxidation for 30 s. The SERS active substrate was prepared by immobilizing 80 nm gold nanoparticles onto the 3-aminopropyltrimethoxysilane (APTMS)-modified glass slide, which was made by the molecular vapor deposition (MVD 100).

### 2.3 Nanofluidic concentration of protein aggregates

To visualize the nanofluidic concentration of protein aggregates, each protein solution was mixed with a 30 μM thioflavin-T (ThT) solution with a volume ratio of 1 : 10 and then each aliquot with a volume of 10 μl was injected into the inlet of a nanofluidic device. After the injected protein sample was flown through the concentrated protein aggregates were observed by imaging with fluorescence microscopy. Our nanofluidic/Raman experiments were carried out after sampling from protein solutions which were incubated *in vitro* outside the device. Protein aggregation itself occurred in free solution with samples taken at the appropriate times (0 day, 2 days, 1 week, and 2 months) for analysis. The device therefore concentrates the already formed protein aggregates to facilitate analysis rather than to drive the aggregation process. This operation is completed in less than 1 hour. Considering that aggregation process *in vivo* as well as *in vitro* is quite slow, it is expected that there is no significant further aggregation during our operation time. For all protein samples including control samples, concentration tests were performed at least two times.

### 2.4 Raman spectroscopic measurements label-free Raman detection of the concentrated protein aggregates

Raman measurements were performed using a Renishaw inVia Raman microscope spectrometer coupled to a Leica microscope by focusing the excitation laser on the concentrated sample. The 785 nm laser was used as a optical excitation source and the scattered signal was collected by a Peltier-cooled CCD detector. A 20× (NA = 0.40) objective lens was used to focus the laser beam spot onto the sample surface. Each Raman spectrum was collected by averaging three consecutive scans. The spectra in the 800–1700 $cm^{-1}$ region were examined here. For the collection of Raman signal generated from only protein aggregates, all spectra were corrected by subtracting a background spectrum.

## 3 Results and discussion

### 3.1 Fabrication of a nanofluidic channels

In our device, sub-micrometre channels are formed by employing our previously reported elastomeric collapse technique

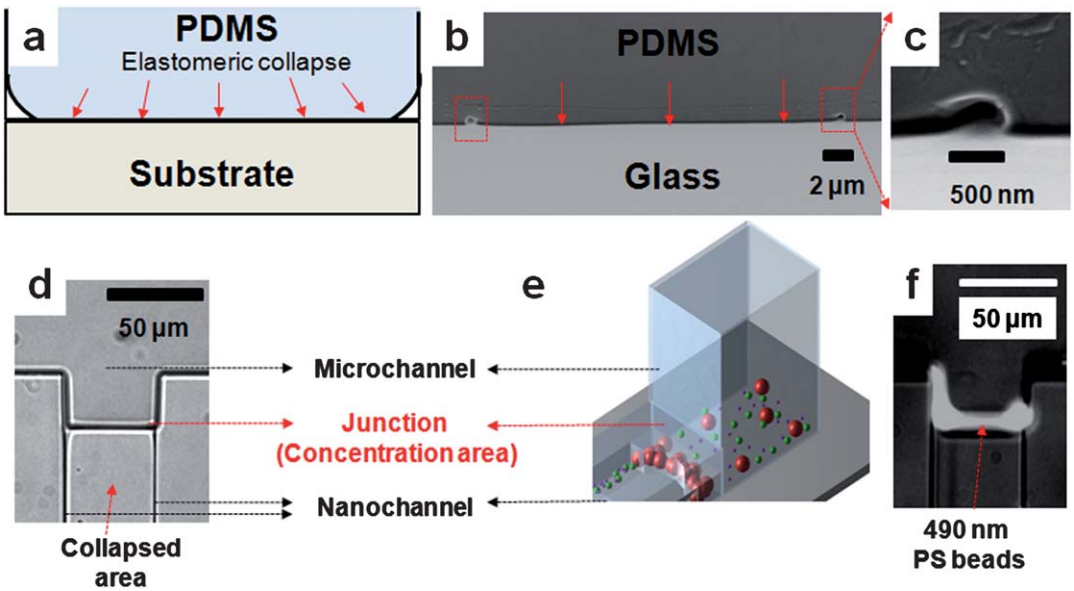


**Fig. 2** Formation and characterization of nanofluidic channels. (a) Schematic diagram to illustrate elastomeric collapse of PDMS. (b) SEM image for a cut plane through the fabricated nanochannels. The two red boxes show the location of the nanochannels formed by the elastomeric collapse method. (c) A magnified image of a nanochannel in (b). (d) A top view of nanofluidic channels formed by PDMS collapse. (e) A three dimensional description of the size-selective concentration process. (f) An image of 490 nm PS beads accumulated at the junction between a microchannel and a nanochannel.

 

(Fig. 2a).[20] Details of the fabrication process are provided in the methods section, but briefly, PDMS microchannels with a predefined aspect ratio (design rules are provided in Park *et al.*[20]) are first fabricated using a patterned master and traditional soft lithography processes. When the PDMS mold is placed in conformal contact with a substrate, the elastomeric nature of the microchannel causes it to sag and eventually collapse with the roof bonding to the lower substrate. Fig. 2b shows a scanning electron microscopy (SEM) image of a cross-section of the formed nanochannels (indicated with two red boxes) following collapse. The red arrows indicate the collapsed area. As shown in Fig. 2c, the dimensions of both the width and the height of the fabricated channel were below 500 nm. The protein aggregates of interest here generally have nanometre scale thickness (for the amorphous case) and/or diameter (for the fibril case), even if they have much larger lateral dimensions (width or length) (Fig. 1d). To form a microfluidic network to feed the protein aggregates into the micro/nanofluidic junctions, the PDMS mold also contained channels with higher aspect ratios, above the threshold at which elastomeric collapse would be expected.[20] Fig. 2d and e show a top view of a fabricated fluidic channels and a three dimensional description of size-selective concentration. Fig. 2f shows the collection of 490 nm fluorescence polystyrene (PS) beads at the junction between the microchannel and nanochannel.

### 3.2 Fabrication of a Raman active nanofluidic device

The use of the elastomeric collapse method greatly facilitates the integration of a SERS active substrate into the device and thereby label-free characterization of protein aggregates (Fig. 3a). In addition, gold nanoparticles immobilized on the surface serve as stable SERS active plasmonic enhancers rather than those in colloidal state. In these experiments we used a SERS active substrate which comprised of gold nanoparticles clusters (Fig. 3b) formed on the glass slide which had been earlier modified with APTMS. To assemble the final device, the PDMS mold was placed onto the immobilized gold nanoparticle clusters and allowed to collapse, as shown in Fig. 3c. The quality of the individual channels was gauged using optical microscopy and SEM as well as control experiments with beads. Optical images allow us to identify the formation and dimensional uniformity of formed nanochannels. SEM images provide precise dimensions of uniformly formed nanochannels. Finally, control experiments with different sized beads (51 nm, 210 nm, and 490 nm, and 1 μm) show highly selective concentration performance of such devices (see Fig. S1, ESI†). Using hydrodynamic sample injection, 490 nm and 1 μm beads were accumulated at the fluidic junctions, while 51 nm and 210 nm beads passed through the channel. On the basis of our all characterization results, we concluded that the uniformity of the devices is sufficient such that new devices could be used for each experiment without the added complication (and potential contamination) associated with attempting to regenerate a device (*i.e.* removal of such as beads or proteins). Moreover, this size-selective concentration and simple pressure driven injection have significant advantages for protein aggregation studies over other recently developed electrokinetic techniques[21–23] as the application of an external electric field can induce unintentional and additional aggregation of proteins.

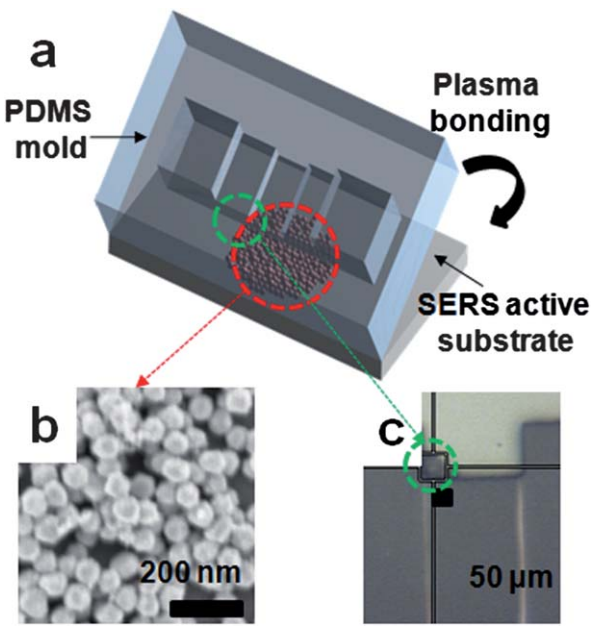


**Fig. 3** Device configuration for label-free detection of concentrated protein aggregates. (a) A schematic diagram showing the integration of the nanofluidic device with the SERS active substrate. (b) An SEM image of a gold nanoparticles cluster immobilized on a glass slide. (c) A top view of a device fabricated by the procedure illustrated in (a).

### 3.3 Validation of size-selective concentration of SOD1 aggregates with a device

The *in vitro* formation of SOD1 aggregates was achieved through treatment with TFE, following a previously reported experimental protocol.[6] TFE has been extensively used to study the aggregation of other proteins.[24,25] The protein aggregation itself occurred in free solution outside the microfluidic device and samples were taken at the appropriate analysis time points (0 day, 2 days, 1 week, and 2 months). After sampling from the protein solutions the following procedures were carried out within the device. To visualize the concentration performance of the device the incubated SOD1 proteins were treated with ThT, a common dye traditionally used to monitor the formation of protein aggregates,[4,6,8] before injection. The insets of Fig. 4 show the representative size-selective concentration of aggregates according to the incubation times of SOD1 at an initial concentration of 300 nM. As can be seen, with increasing incubation time the amount of protein aggregates trapped by the device also increases due to the existence of a greater number of protein aggregates with sizes over the width and height of a nanochannel. Protein aggregates were not observed at the initial state (0 day), as the expected structures comprise primarily of monomers and/or small oligomers. Since large protein aggregates are mixed with these small protein species (monomers, oligomers, and small aggregates) with a different number distribution at each characterization time point (see Fig. 1d), this incubation time concentration performance test at same initial protein concentration validates the size-selective concentration capability of our device. As control tests, we performed additional experiments with freshly prepared monomers including

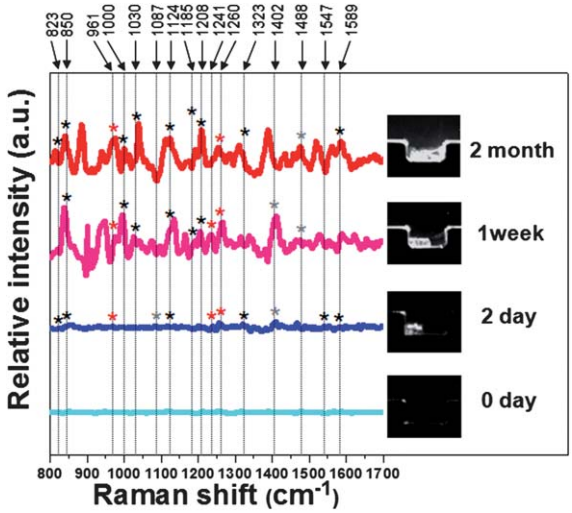


**Fig. 4** A proof-of-concept test for label-free detection of concentrated protein aggregates. SERS spectra of protein aggregates with different incubation times (2 month, 1 week, 2 day, and 0 day). The initial protein concentration was 300 nM. In the spectra, remarkable peaks indicated with black asterisks are related to hydrophobic residues. Gray asterisks indicate charged and hydrophilic residues. Red asterisks represent the most noticeable changes (*i.e.* secondary structures and surface hydrophobicity) in proteins during the aggregation process. Insets show florescent images of the protein aggregates concentrated at the micro/nanofluidic junctions.

SOD1 monomer and bovine serum albumin monomers. In these cases, we did not observe any protein concentration at the junction between the microchannel and the nanochannel (*i.e.* the small monomers were able to pass through the nanochannels). For all cases, most of protein aggregates were concentrated within several minutes.

Fig. 4 also shows the Raman spectra, in the spectral range of 800–1700 $cm^{-1}$, collected for each of the concentrated SOD1 aggregates. Consistent with the fluorescence results, these spectra reveal the existence of SOD1 aggregates in all cases except for the 0 day sample. In the Raman spectra, remarkable peaks (see Table S1, ESI†) indicated with black asterisks are related to hydrophobic residues (*i.e.* phenylalanine, valine, and isoleucine). Gray asterisks indicate charged and hydrophilic residues (*i.e.* lysine, arginine, glutamine, asparagine, aspartic acid, glutamic acid, and histidine). The red marked peaks represent the most noticeable changes (*i.e.* secondary structures and surface hydrophobicity) in proteins during the aggregation process. As will be expanded on later, the changes in the spectra for the different incubation times can be attributed to conformational changes of protein aggregates.

### 3.4 Label-free Raman characterization of SOD1 aggregates at low concentrations

Having established that our device can separate, concentrate and detect protein aggregates with disease implication from the native protein, we further applied this device to quantify concentration dependent protein aggregation. SOD1 aggregates were prepared at wide concentration ranges (from 3 fM to 300 nM) and then they were injected into devices to separate the matured aggregates from small oligomers or monomers. As can be seen in Fig. S2a†, we clearly observed differences in the amount of aggregates as a function of the initial protein concentration at levels as low as 3 fM. This is well below that which can be distinguished using traditional fluorescence methods which have μM level limits of detection (see Fig. S2b, ESI†). This is attributable to the ability of our device to directly collect protein aggregates in the confined area to be measured. Non-uniform distribution of protein aggregates (see the inset of Fig. S2b, ESI†) can result in an inaccurate measurement in the case of other solution-based analysis techniques. To overcome this, our size-selective concentration experiments were carried out with Raman active nanofluidic devices to concentrate the already formed protein aggregates and to facilitate further analysis of them. Size-selective concentration results, showing that the amount of protein aggregates trapped increases with the increase of initial concentration, support the high selectivity of our system for aggregates, since the amount of protein aggregates formed generally increases with initial concentrations of protein monomers. We performed size-selective concentration experiments with a device for protein aggregates incubated under different initial concentrations several times and results show high reproducibility.

Fig. 5a shows the Raman spectra of protein aggregates concentrated from samples incubated for 47 days at different initial concentrations. The structural significance of the observed Raman bands was identified on the basis of existing literature pertaining to the spectra of amino acids and proteins.[26–31] Table S1† summarizes the Raman bands of relevance here (*i.e.* aromatic rings, carboxylic group vibrations, and amide III region). Compared to the band assigned for SOD1 in the literature,[29,30] the slight shifts observed here can be attributed to the alteration induced by protein–metal interactions. Prior to collection of spectra from the protein aggregates, signal quality was checked by taking spectra in the areas of the chip where protein aggregates were not trapped, that is, composed of only nanoparticle clusters. These control spectra were nearly identical at all locations and no significant Raman peaks were observed (as in the control spectrum shown in Fig. 5a). For the protein samples, all spectra were corrected by subtracting this control spectrum from the collected Raman signal.

Compared to the control spectrum, we observed specific Raman bands generated from the protein aggregates for concentrations greater than 3 fM. Although the intensity of the band observed for 3 fM sample is weak, it is sufficient to identify the existence of protein aggregation. At this low concentration (3 fM), we observed Raman bands associated with the aromatic side chains at 1185 $cm^{-1}$ (phenylalanine, tyrosine). The presence of these bands indicates that the aromatic side chains are in a favorable position with respect to the gold nanoparticle surface. The band at 1402 $cm^{-1}$ corresponds to that for the carboxyl group and may be due to the aspartate residue which is consistent with the presence of zinc ions in the SOD1.[29] Most prominently at low concentrations, the two bands at 1241 $cm^{-1}$ and 1260 $cm^{-1}$ (in the amide III region) suggest that SOD1 has both β-sheet structure and α-helix structure. Note that the secondary structure of ordered SOD1 is known to be mainly comprised of 60% β-sheet and 30% random coil with the remainder being an α-helix.[4,32]

 

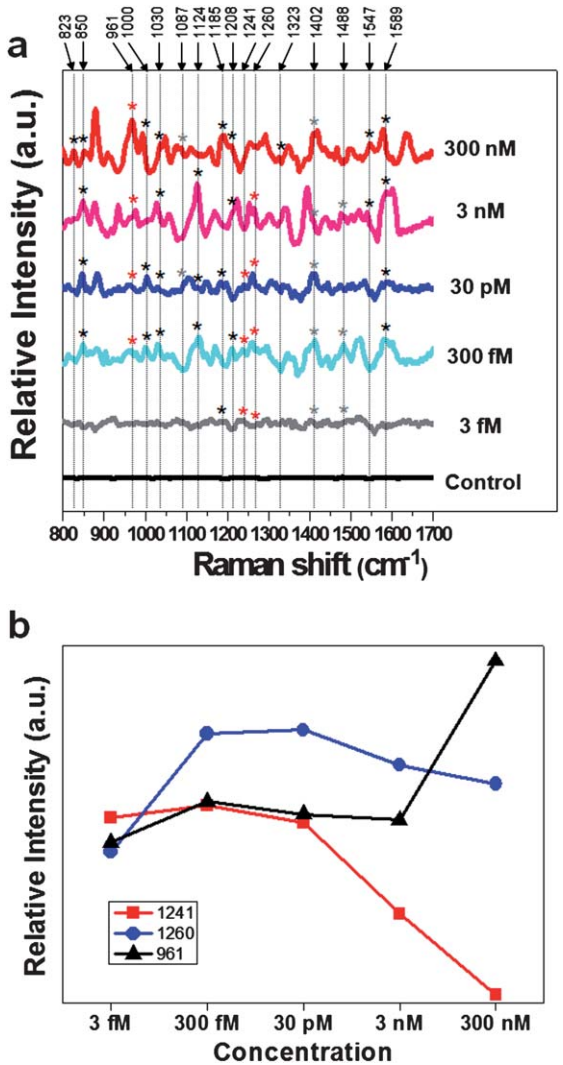


**Fig. 5** Raman characterization of concentration dependent SOD1 aggregation. (a) SERS spectra of SOD1 aggregates concentrated at micro/nanofluidic junctions. SOD1 aggregates were prepared for concentration ranges from 3 fM to 300 nM and incubated for 47 days. Three consecutive scans were performed for all samples. A control spectrum was collected for the areas where nanoparticle clusters exist but no protein aggregates are trapped. (b) A plot for concentration dependent relative intensity at several peaks, which were closely associated with the secondary structures (1241 $cm^{-1}$ and 1260 $cm^{-1}$) and surface properties (961 $cm^{-1}$).

### 3.5 Interpretation of concentration dependent SOD1 aggregation from Raman detection

As a concentration increases, peak shifts were observed at each spectrum. It should be noted that signal intensities of all Raman peaks are not usually correlated with protein concentrations, since Raman signatures tend to depend on the extent of protein aggregation and its resulting conformation. As shown in Fig. 5, the band at 1241 $cm^{-1}$ clearly diminishes while slightly changing a band at 1260 $cm^{-1}$ at a higher intensity. Above a concentration of 3 nM, the 1241 $cm^{-1}$ band is hidden in the spectrum. This is a good indication that the polypeptide backbones of the SOD1 aggregates begin to take on a different conformation in close vicinity to the nanoparticle surface, as the aggregation progresses. It should be noted that changes in the amide III region, 1200–1300 $cm^{-1}$, reflect the most compelling changes in proteins and are widely used to quantitatively explore secondary structure.[26–31] Therefore, the changes in the relative intensity between the peak around 1240 $cm^{-1}$ and the peak around 1260 $cm^{-1}$ provide information about the prevalence of α-helix and β-sheet structures. Fig. 5b shows a plot for concentration dependent relative intensity at a number of important peaks, which were closely associated with secondary structures and surface properties. Since β-sheet structure is a main secondary structure of native SOD1, the decrease of the band at 1241 $cm^{-1}$ indicates that SOD1s undergo conformational changes under destabilizing conditions and consequently lose their original structural orderness. This result is consistent with other reports that SOD1 usually forms disordered amorphous structures rather than ordered fibrillar structure.[1,6,15–17] The amorphousness of the SOD1 aggregates was confirmed by imaging morphologies (Fig. 1d) and analyzing secondary structures using CD spectroscopy (see Fig. S3a, ESI†). Additionally, the increase of the band at 961 $cm^{-1}$ (assigned to the C–C stretching in the hydrophobic segment of polypeptide backbone) can be attributed to the increase of hydrophobicity of protein surface (see Fig. S3b, ESI†),[31] since the conformational changes in proteins are generally accompanied by structural turnover and/or changes in surface residues. This is also directly correlated with the spectra showing that a large number of bands associated with hydrophobic residues (black asterisks) are prominently observed with increasing concentration.

Using our device we have observed that aggregation propensity is strongly related with its initial concentration over the range from very low (3 fM) to relatively high concentration (300 nM). Although some researchers have suggested that increasing the protein concentration would result in conformational changes associated with aggregation,[1,5,9,33] the examination of SOD1 aggregation at concentrations used in these studies is an unprecedented analysis, because of the limits of existing analytical tools used for structure determination (*i.e.* CD spectroscopy,[4,7–9] NMR spectroscopy[9–11] and, traditional Raman spectroscopy[27] are usually operated with samples of over μM concentrations). The present SERS studies demonstrate the ability to provide information on structural and surface properties of protein aggregates at a very low concentration, and consequently provide great potential in early stage diagnosis with a sparse population of protein aggregates. Since the evanescent field of the plasmon wave decays rapidly, it allows us to primarily collect signals from the surface of the protein aggregates. Therefore, the spectra we collect here provide abundant information on the surface properties (*e.g.* overall hydrophobicity and exposed surface residues) as well as secondary structural prevalence (*e.g.* α-helix and β-sheet) of the protein aggregates according to their incubation conditions. To confirm the versatility of the approach, we performed a similar analysis using amyloid-β (Aβ), which is implicated in AD and usually forms fibrillar structures. Analogous results were also obtained for Aβ aggregates, as shown in Fig. S4†. In this case, as Aβ aggregation progresses, the increase of β-sheet structures (opposite result of the SOD1 aggregation), which is a general property of Aβ aggregates, was observed by Raman characterization (data not shown).

## 4 Conclusions and summary

In conclusion, our method represents a powerful approach to study protein aggregation, since it is capable of providing structural information of proteins in various states: soluble (or insoluble) aggregates, fibrillar (or non-fibrillar and amorphous) aggregates and crystalline (or non-crystalline) aggregates. This is attributable to the capability of a nanofluidic concentration device to separate and concentrate the protein aggregates irrespective of their solubility, morphology, and crystallinity. Additionally, analysis of protein amide III band profiles provides information on the composition of secondary structures (α-helix and β-sheet), and the Raman spectra reveal several sensitive markers of exposed protein surface residues according to the aggregation status. To the best of our knowledge, this amount of information could not have been obtained using traditional methods (*e.g.* CD spectroscopy, NMR spectroscopy, X-ray crystallography, and fluorescence spectroscopy combined with specific dyes) for small amount of protein samples.

In summary, we have demonstrated a nanofluidic concentration-based Raman detection system that can semi-quantitatively and qualitatively characterize protein aggregates. Nanofluidic concentration enables us to detect the trace amounts of protein aggregates with disease implications at a very low concentration. Simultaneously, label-free Raman characterization of protein aggregates allows the investigation of the changes in intrinsic properties during the protein aggregation. Collectively, our findings allow us to comprehensively understand the surface and structural properties of the protein aggregates according to their aggregation stage. This approach provides the potential for definitive diagnosis and possible therapeutics of protein conformational diseases at early states.

## Acknowledgements

The authors acknowledge funding from and access to the facilities of the Nanobiotechnology Center (NBTC), an STC Program of the National Science Foundation under Agreement no. ECS-9876771. The authors also appreciate access and use of the Cornell Nanoscale Science and Technology Facility (a member of the National Nanofabrication Users Network), which is supported by the National Science Foundation under grant ECS-9731293. I.C. was partially supported by a grant from the National Research Foundation of Korea Grant funded by the Korean Government [NRF-2009-352-D00053].

## References

1 C. A. Ross and M. A. Poirier, *Nat. Med.*, 2004, **10**, S10–S17.
2 R. R. Kopito, *Trends Cell Biol.*, 2000, **10**, 524–530.
3 H. A. Lashuel, *Sci. Aging Knowl. Environ.*, 2005, **2005**, pe28.
4 L. Banci, I. Bertini, A. Durazo, S. Girotto, E. B. Gralla, M. Martinelli, J. S. Valentine, M. Vieru and J. P. Whitelegge, *Proc. Natl. Acad. Sci. U. S. A.*, 2007, **104**, 11263–11267.
5 S. D. Khare, M. Caplow and N. V. Dokholyan, *Proc. Natl. Acad. Sci. U. S. A.*, 2004, **101**, 15094–15099.
6 P. B. Stathopulos, J. A. O. Rumfeldt, G. A. Scholz, R. A. Irani, H. E. Frey, R. A. Hallewell, J. R. Lepock and E. M. Meiering, *Proc. Natl. Acad. Sci. U. S. A.*, 2003, **100**, 7021–7026.
7 R. Rakhit, J. P. Crow, J. R. Lepock, L. H. Kondejewski, N. R. Cashman and A. Chakrabartty, *J. Biol. Chem.*, 2004, **279**, 15499–15504.
8 Y. Furukawa, K. Kaneko, K. Yamanaka, T. V. O'Halloran and N. Nukina, *J. Biol. Chem.*, 2008, **283**, 24167–24176.
9 L. Banci, I. Bertini, N. D'Amelio, E. Gaggelli, E. Libralesso, I. Matecko, P. Turano and J. S. Valentine, *J. Biol. Chem.*, 2005, **280**, 35815–35821.
10 L. Banci, I. Bertini, M. Boca, V. Calderone, F. Cantini, S. Girotto and M. Vieru, *Proc. Natl. Acad. Sci. U. S. A.*, 2009, **106**, 6980–6985.
11 K. H. Lim, Y. K. Kim and Y. T. Chang, *Biochemistry*, 2007, **46**, 13523–13532.
12 M. Sutter, S. Oliveira, N. N. Sanders, B. Lucas, A. van Hoek, M. A. Hink, A. J. W. G. Visser, S. C. De Smedt, W. E. Hennink and W. Jiskoot, *J. Fluoresc.*, 2007, **17**, 181–192.
13 J. Behlke and A. Knespel, *J. Cryst. Growth*, 1996, **158**, 388–391.
14 P. L. Stiles, J. A. Dieringer, N. C. Shah and R. R. Van Duyne, *Annu. Rev. Anal. Chem.*, 2008, **1**, 601–626.
15 B. F. Shaw and J. S. Valentine, *Trends Biochem. Sci.*, 2007, **32**, 78–85.
16 G. Matsumoto, A. Stojanovic, C. I. Holmberg, S. Kim and R. I. Morimoto, *J. Cell Biol.*, 2005, **171**, 75–85.
17 S. Sasaki, H. Warita, T. Murakami, N. Shibata, T. Komori, K. Abe, M. Kobayashi and M. Iwata, *Acta Neuropathol.*, 2005, **109**, 247–255.
18 E. M. Meiering, *PLoS Biol.*, 2008, **6**, e193.
19 H. X. Deng, Y. Shi, Y. Furukawa, H. Zhai, R. G. Fu, E. D. Liu, G. H. Gorrie, M. S. Khan, W. Y. Hung, E. H. Bigio, T. Lukas, M. C. Dal Canto, T. V. O'Halloran and T. Siddique, *Proc. Natl. Acad. Sci. U. S. A.*, 2006, **103**, 7142–7147.
20 S. M. Park, Y. S. Huh, H. G. Craighead and D. Erickson, *Proc. Natl. Acad. Sci. U. S. A.*, 2009, **106**, 15549–15554.
21 S. M. Kim, M. A. Burns and E. F. Hasselbrink, *Anal. Chem.*, 2006, **78**, 4779–4785.
22 A. Plecis, C. Nanteuil, A. M. Haghiri-Gosnet and Y. Chen, *Anal. Chem.*, 2008, **80**, 9542–9550.
23 J. H. Lee, Y. A. Song, S. R. Tannenbaum and J. Han, *Anal. Chem.*, 2008, **80**, 3198–3204.
24 M. Calamai, C. Canale, A. Relini, M. Stefani, F. Chiti and C. M. Dobson, *J. Mol. Biol.*, 2005, **346**, 603–616.
25 K. Yamaguchi, S. Takahashi, T. Kawai, H. Naiki and Y. Goto, *J. Mol. Biol.*, 2005, **352**, 952–960.
26 C. Ortiz, D. M. Zhang, Y. Xie, V. J. Davisson and D. Ben-Amotz, *Anal. Biochem.*, 2004, **332**, 245–252.
27 N. C. Maiti, M. M. Apetri, M. G. Zagorski, P. R. Carey and V. E. Anderson, *J. Am. Chem. Soc.*, 2004, **126**, 2399–2408.
28 J. Dong, C. S. Atwood, V. E. Anderson, S. L. Siedlak, M. A. Smith, G. Perry and P. R. Carey, *Biochemistry*, 2003, **42**, 2768–2773.
29 J. R. Lepock, L. D. Arnold, B. H. Torrie, B. Andrews and J. Kruuv, *Arch. Biochem. Biophys.*, 1985, **241**, 243–251.
30 S. Hashimoto, K. Ono and H. Takeuchi, *J. Raman Spectrosc.*, 1998, **29**, 969–975.
31 I. H. Chou, M. Benford, H. T. Beier, G. L. Cote, M. Wang, N. Jing, J. Kameoka and T. A. Good, *Nano Lett.*, 2008, **8**, 1729–1735.
32 H. Nagami, N. Yoshimoto, H. Umakoshi, T. Shimanouchi and R. Kuboi, *J. Biosci. Bioeng.*, 2005, **99**, 423–428.
33 W. Jiang, Y. C. Han, R. Y. Zhou, L. N. Zhang and C. L. Liu, *Biochemistry*, 2007, **46**, 5911–5923.

 